SPECIAL FEATURE

Multisectoral climate impact hotspots in a warming world

Franziska Piontek[a,1], Christoph Müller[a], Thomas A. M. Pugh[b], Douglas B. Clark[c], Delphine Deryng[d], Joshua Elliott[e], Felipe de Jesus Colón González[f], Martina Flörke[g], Christian Folberth[h], Wietse Franssen[i], Katja Frieler[a], Andrew D. Friend[j], Simon N. Gosling[k], Deborah Hemming[l], Nikolay Khabarov[m], Hyungjun Kim[n], Mark R. Lomas[o], Yoshimitsu Masaki[p], Matthias Mengel[a], Andrew Morse[q], Kathleen Neumann[r,s], Kazuya Nishina[p], Sebastian Ostberg[a], Ryan Pavlick[t], Alex C. Ruane[u], Jacob Schewe[a], Erwin Schmid[v], Tobias Stacke[w], Qiuhong Tang[x], Zachary D. Tessler[y], Adrian M. Tompkins[f], Lila Warszawski[a], Dominik Wisser[z], and Hans Joachim Schellnhuber[a,aa]

[a]Potsdam Institute for Climate Impact Studies, Potsdam 14473 Germany; [b]Institute of Meteorology and Climate Research, Atmospheric and Environmental Research, Karlsruhe Institute of Technology, 82467 Garmisch-Partenkirchen, Germany; [c]Centre for Ecology and Hydrology, Wallingford OX1 08BB, United Kingdom; [d]School of Environmental Sciences, Tyndall Centre, University of East Anglia, Norwich NR4 7TJ, United Kingdom; [e]University of Chicago Computation Institute, Chicago, IL 60637; [f]Abdus Salam International Centre for Theoretical Physics, 34151 Trieste, Italy; [g]Center for Environmental Systems Research, University of Kassel, 34109 Kassel, Germany, [h]Swiss Federal Institute of Aquatic Science and Technology (EAWAG), 8600 Dübendorf, Switzerland; [i]Earth System Science, Wageningen University, 6708PB, Wageningen, The Netherlands; [j]Department of Geography, University of Cambridge, Cambridge CB2 1TN, United Kingdom; [k]School of Geography, University of Nottingham, Nottingham NG7 2RD, United Kingdom; [l]Met Office Hadley Centre, Exeter EX1 3PB, United Kingdom; [m]International Institute for Applied Systems Analysis, 2361 Laxenburg, Austria; [n]Institute of Industrial Science,University of Tokyo, Tokyo 153-8505, Japan; [o]Department of Animal and Plant Sciences, University of Sheffield, Sheffield S10 2TN, United Kingdom; [p]Center for Global Environmental Research, National Institute for Environmental Studies, Tsukuba 305-8506, Japan; [q]School of Environmental Sciences, University of Liverpool, Liverpool L69 3GP, United Kingdom; [r]PBL Netherlands Environmental Assessment Agency, 3720 AH Bilthoven, The Netherlands; [s]Rural Development Sociology, Wageningen University, 6706 KN Wageningen, The Netherlands; [t]Max Planck Institute for Biogeochemistry, 07745 Jena, Germany, [u]National Aeronautics and Space Administration Goddard Institute for Space Studies, New York, NY 10025; [v]Department for Economic and Social Sciences, University of Natural Resources and Life Sciences, 1180 Vienna, Austria, [w]Max Planck Institute for Meteorology, 20146 Hamburg, Germany, [x]Institute of Geographic Sciences and Natural Resources Research, Chinese Academy of Sciences, Beijing 100101, China, [y]City University of New York Environmental CrossRoads Initiative, City College of New York, New York, NY 10031; [z]Department of Physical Geography, Utrecht University, 3508 TC Utrecht, The Netherlands; and [aa]Santa Fe Institute, Santa Fe, NM 87501

Edited by Robert W. Kates, Independent Scholar, Trenton, ME, and approved June 4, 2013 (received for review January 31, 2013)

The impacts of global climate change on different aspects of humanity's diverse life-support systems are complex and often difficult to predict. To facilitate policy decisions on mitigation and adaptation strategies, it is necessary to understand, quantify, and synthesize these climate-change impacts, taking into account their uncertainties. Crucial to these decisions is an understanding of how impacts in different sectors overlap, as overlapping impacts increase exposure, lead to interactions of impacts, and are likely to raise adaptation pressure. As a first step we develop herein a framework to study coinciding impacts and identify regional exposure hotspots. This framework can then be used as a starting point for regional case studies on vulnerability and multifaceted adaptation strategies. We consider impacts related to water, agriculture, ecosystems, and malaria at different levels of global warming. Multisectoral overlap starts to be seen robustly at a mean global warming of 3 °C above the 1980–2010 mean, with 11% of the world population subject to severe impacts in at least two of the four impact sectors at 4 °C. Despite these general conclusions, we find that uncertainty arising from the impact models is considerable, and larger than that from the climate models. In a low probability-high impact worst-case assessment, almost the whole inhabited world is at risk for multisectoral pressures. Hence, there is a pressing need for an increased research effort to develop a more comprehensive understanding of impacts, as well as for the development of policy measures under existing uncertainty.

coinciding pressures | differential climate impacts | ISI-MIP

Over the coming decades, climate change is likely to significantly alter human and biological systems, pushing the boundaries of variability beyond historic values and leading to significant changes to what are considered typical conditions. Identifying the locations, timings, and features of these impacts for a given level of global warming in advance allows the development of appropriate adaptation strategies, or can motivate decisions to mitigate climate change. Although climate-change impacts are extensively studied in individual sectors, their overlaps and interactions are rarely taken into account. However, these impacts are likely to be of great consequence, as they can amplify effects, restrict response options, and lead to indirect impacts in other regions, thus strongly increasing the challenges to adaptation (1). In this article we take an important first step toward the analysis of these effects through a consistent assessment of the geographical coincidence of impacts as multisectoral exposure hotspots. The Intersectoral Impact Model Intercomparison Project (ISI-MIP, www.isi-mip.org) offers a unique opportunity for this analysis by providing multimodel ensembles of climate-change impacts across different sectors in a consistent scenario framework.

Through the investigation of biophysical impacts of climate change, which form the linkage between climate and society (2, 3), this study moves beyond previous hotspot analyses that have mostly used purely climatic indicators (4–7). In addition, the setup enables an assessment of uncertainty because of both multiple Global Climate Models (GCMs) and multiple Global Impact Models (GIMs) in each sector (8). Finally, impacts are analyzed at different levels of global mean temperature (GMT) for a comparison at different levels of global warming. This global analysis serves two objectives. First, tangible adaptation strategies require knowledge of local vulnerability, defined by exposure, sensitivity, and adaptive capacity. The regional exposure hotspots can therefore serve as a starting point for prioritized case studies and studies of interactions as the basis for the development of adaptation strategies that can be expanded to additional regions as needed. Second, the focus on GMT change is crucial when studying costs and benefits of mitigation policies,

Author contributions: F.P., K.F., J.S., L.W., and H.J.S. designed research; F.P. performed research; F.P., C.M., T.A.M.P., D.B.C., D.D., J.E., F.d.J.C.G., M.F., C.F., W.F., A.D.F., S.N.G., D.H., N.K., H.K., M.R.L., Y.M., M.M., A.M., K. Neumann, K. Nishina, S.O., R.P., A.C.R., E.S., T.S., Q.T., Z.D.T., A.M.T., and D.W. analyzed data; and F.P., C.M., and T.A.M.P. wrote the paper.

The authors declare no conflict of interest.

This article is a PNAS Direct Submission.

[1]To whom correspondence should be addressed. E-mail: piontek@pik-potsdam.de.

This article contains supporting information online at www.pnas.org/lookup/suppl/doi:10.1073/pnas.1222471110/-/DCSupplemental.

such as the 2 °C target set by the international community to reduce risks from climate-change impacts and damages (9, 10).

The analysis comprises four key impact sectors: water, agriculture, ecosystems, and health. Health is represented by malaria, which, albeit being only one example of health impacts of climate change, does have potentially severe economic consequences (11). As metrics for the four sectors, we select river discharge as a measure of water availability, crop yields for four major staple crops (wheat, rice, soy, and maize) on currently rain-fed and irrigated cropland (12) (Fig. S1), the ecosystem change metric Γ (13), and the length of transmission season (LTS) for malaria. Although these four metrics do not cover the full range of possible societally relevant climate-change impacts, they do include crucial aspects of livelihoods and natural resources, especially for developing countries: water availability, food security, ecosystem stability, and a key health threat.

We aim to define levels of change in each sector that can be considered severe as basis for multisectoral hotspots. "Severe" is taken to mean a shift of average conditions across selected thresholds representing significant changes relative to the historical norm. A multisectoral perspective is thus possible through the simultaneous occurrence of above-threshold changes in multiple sectors. Although climate change can have both positive and negative impacts, for the purpose of vulnerability analysis we identify hotspots of changes that put additional stresses on human and biological systems. Average conditions are measured as the median over 31-y time periods. For the thresholds, we take a statistical approach for water availability and crop yields, whereas we use a more comprehensive metric for ecosystem change, and resort to a relatively simple indicator for malaria conditions. The thresholds in the water and agricultural sectors are defined as the 10th percentile of the reference period distribution (1980–2010) of discharge and crop yields, respectively. This threshold means a shift of average conditions into what is considered today moderately extreme, happening in only 10% of all years. Behavior is robust to the choice of a smaller threshold (Fig. S2). This low end of the distribution excludes floods, as the focus is on reduced water availability. Clearly, the chance to cross the threshold depends on the level of variability in a given region and may in fact mean relatively small absolute change; however, it reflects the assumption that people in regions already subject to highly variable conditions are better prepared to adapt to more extreme average conditions (14).

The Γ-metric (13) represents the difference between future states of ecosystems and present day conditions through an aggregate measure of changes in stores and fluxes of carbon and water, as well as vegetation structures. A large value of Γ indicates significant changes in biogeochemical conditions or vegetation structure, which would likely lead to considerable transformations of the ecosystem. Based on differences between present day ecosystems, Heyder et al. (13) define $\Gamma > 0.3$ as the threshold for a risk of severe change, [see also *SI Text* and Warszawski et al. (15)]. Such changes may reduce biodiversity, which is crucial for the resilience of many ecosystem services (16). Furthermore, the livelihoods of many vulnerable populations, along with cultural values and traditions, are closely tied to existing ecosystems (17). The threshold for changes in the prevalence of malaria is defined as a shift in the LTS, from < 3 mo to >3 mo. This shift corresponds approximately to a switch from epidemic to endemic malaria based on climatic conditions (based on data from the Mapping Malaria Risk in Africa project, www.mara.org.za) (Fig. S3).

All impacts are simulated with multiple, predominantly process-based GIMs (agriculture and ecosystems, 7 models each; water, 11 models; malaria, 4 models). These GIMs are driven by three GCMs, simulating the highest representative concentration pathway (RCP8.5) (18). Although current emissions are following a similar trajectory, we choose RCP8.5 primarily to cover the largest possible temperature range, not as a worst-case scenario (19). For each GIM-GCM combination and at each grid point, we define a "crossing temperature" that is the GMT change (ΔGMT) at which the sectoral metric crosses the respective impact threshold. Sectoral crossing temperatures are then taken as the median over all GIM-GCM combinations of a given sector. In our strict assessment, only robust results are taken into account, defined as an agreement of at least 50% of all GIM-GCM combinations of a given sector at which the threshold is crossed. Overlapping pressures at a given grid point are assumed to arise when multiple sectors have crossed at a given ΔGMT. Results are presented in terms of total area affected by the shift as a function of ΔGMT. Note that GMT changes in this report are with respect to the 1980–2010 period, which is ∼0.7 °C above preindustrial levels (20).

Results and Discussion

Sectoral Analysis. The basis for the study of multisectoral overlap is the ΔGMT level at which the thresholds for severe change are crossed (if at all) in each of the four sectors (Fig. 1 and Fig. S4). Median 31-y water availability is projected to drop below the reference distribution's 10th percentile in the Mediterranean, regions of South America, in particular the southern Amazon basin, regions in coastal western and central Africa, and parts of south-central Asia for a warming of up to 4.5 °C under RCP8.5. This distribution includes some regions of large projected relative drop in discharge (21), although the relatively strict 10th percentile criterion means that it does not capture all of them (e.g., southern United States). The regions affected by crop yields below the threshold are tropical regions dominated by rain-fed agriculture; this is consistent with the expectation that rain-fed systems are likely to see larger and more consistent yield losses than irrigated areas that can adapt more successfully. No negative effects on yields are seen at higher latitudes, as these initially benefit from higher temperatures and CO_2 fertilization effects and exhibit yield increases (22). For both discharge and yields, thresholds start to be crossed at ΔGMT = 1 °C.

Significant risk of ecosystem change, as indicated by the Γ-metric, has the largest geographical extent of all sectors, with most regions exhibiting crossing temperatures of 3–4 °C. This large extent occurs because it encompasses very different ecosystem responses, depending on the region and the model. There is forest die-back because of less rainfall in the Amazon and heat stress in boreal forest regions, but also increased greening in Europe and Africa because of warmer, wetter conditions, as well as replacement of some vegetation species with others better adapted to the new conditions. Forest advances northward as a result of higher temperatures and the trees' increased water-use efficiency in response to higher atmospheric CO_2 concentrations. On the Tibetan Plateau, distinguished by the lowest crossing temperature of ΔGMT = 2 °C, increased vegetation growth because of longer growing seasons and warmer winters puts the current grass and shrublands at risk. Although not all of these changes will be negative per se, they would constitute a disruption and possibly a need for adaptation of local societies to the prevailing ecosystem conditions.

Finally, malaria prevalence is expected to increase in higher latitudes, higher altitudes, and in regions on the fringes of current malaria regions because of warmer and wetter climatic conditions. However, when conditions become drier, prevalence can also decrease. As a result of the very different parameterizations used in the four malaria models considered here, agreement among models on the changes is poor, leaving very few areas as robustly crossing the 3-mo LTS threshold. Nevertheless, in agreement with previous work, the Ethiopian Highlands are one of these regions (23).

Multisectoral Hotspots. We define hotspots as regions of multisectoral exposure where two or more of the sectoral metrics have

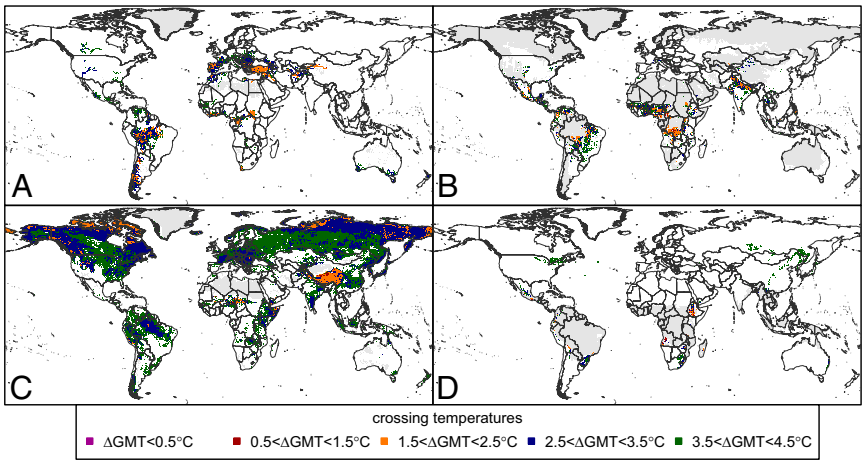

Fig. 1. Threshold crossing temperatures with respect to the reference period GMT for the four sectoral metrics: discharge (*A*), crop yields (*B*), risk of severe ecosystem change (*C*), and LTS of malaria (*D*). Areas in white do not cross the respective threshold. The gray color indicates regions which are either masked out [discharge, Γ, crop yields (only regions where the maize, wheat, soy, and rice are currently cultivated are considered)], or where malaria is already endemic (*D*). An agreement of 50% of all GIM-GCM combinations on threshold crossing is required for consideration in the analysis.

crossed their respective thresholds of severe change in average conditions under the strict assessment, which means with high likelihood (Fig. 2). According to our results there is no overlap of severe change in all four sectors. The most prominent hotspot is the southern Amazon basin, with some parts projected to experience severe changes in three sectors (yields, ecosystems, and discharge) and large areas affected by two pressures. The second largest hotspot region is southern Europe, with overlapping changes in discharge and ecosystems. These two areas, as well as smaller tropical hotspot regions in Central America and Africa, were also identified in other studies using different methods, supporting our findings (5, 6). In addition, we identify the Ethiopian highlands as a hotspot because of the overlap of malaria extension, crop yield reduction, and ecosystem change; northern regions of south Asia are affected by either reductions in discharge and crop yields or crop yield reduction and ecosystem change. These multisectoral hotspots occur in both regions with high population density (i.e., Europe, east Africa, south Asia) and sparsely populated areas (i.e., Amazon). These hotspots cover developed, emerging, and developing economies, each with different degrees of adaptive capacity and sensitivity to the multisectoral pressures. Note that these factors are not taken into account here. A weighting of the relative importance of the sectoral pressures depends strongly on local factors, such as societal structures and values, economic base, and environmental imperatives. Therefore, a more detailed interpretation of the hotspots requires in-depth regional case studies, but is beyond the scope of this study.

Regions typically expected as high-exposure regions, like Africa, do not emerge strongly as hotspots here, which is partially because of the sectors used in the analysis and the individual characteristics of the sectoral metrics, both influencing their combination. In particular, the global area where three or four regions can potentially overlap is limited to where the four staple crops are currently cultivated and where malaria is not yet endemic (excluding gray areas in Fig. 1). Hence, a different picture might arise if, for example, changes in the occurrence of extreme events, like droughts and floods, were included as metrics, which would likely increase the occurrence of hotspots in Africa and south-east Asia (24).

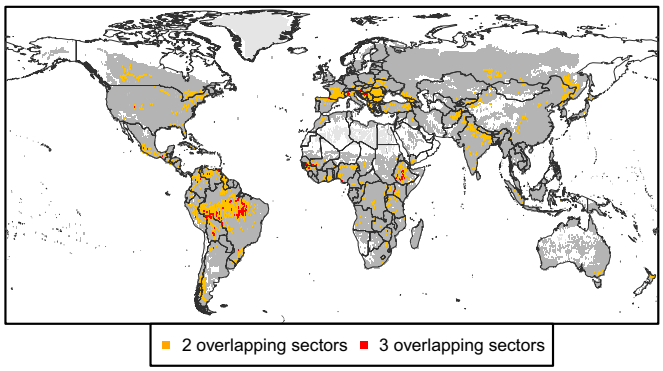

Fig. 2. Multisectoral hotspots of impacts for two (orange) and three (red) overlapping sectors in the strict assessment, with 50% of GIM-GCM combinations agreeing on the threshold crossing in each sector, for a GMT change of up to 4.5 °C. Which sectors overlap depends on the location and can be discerned from the sectoral patterns in Fig.1. An overlap of all four sectors does not occur in the strict assessment. Regions in light gray are regions where no multisectoral overlap is possible at all because of sectoral restrictions as shown in Fig.1. The dark gray shows the additional regions affected by multisectoral pressures under the worst-case assessment, where a minimum of 10% of all sectoral GIM-GCM combinations have to agree on the threshold crossing.

The Role of Uncertainty. An additional factor limiting the overlap of areas with severe change in different sectors is the large uncertainty in projections, stemming mainly from the GCMs and GIMs. When the results for the three GCMs are separated, different multisectoral hotspot patterns emerge, with some regions only appearing as hotspots with a single GCM (Fig. S5). This appearance is because of different sectoral patterns associated with each GCM as a result of variances in projections of key climate variables influencing the impact models. Climate model uncertainty is therefore an important cause of the limited sectoral overlap in our analysis. Uncertainty from impact models, however, is much larger (Fig. 3 and Fig. S2). This finding is in agreement with previous literature and other analyses in this Special Features issue of PNAS (21, 25). Agreement is highest among the ecosystem models, whereas differences are largest between the global crop models. In addition to uncertainty as to whether the thresholds are crossed, there is also uncertainty on the crossing temperature, with SDs of around 1 °C in most sectors (Fig. S6). The details of the model differences are beyond the scope of this report. However, we emphasize the importance of

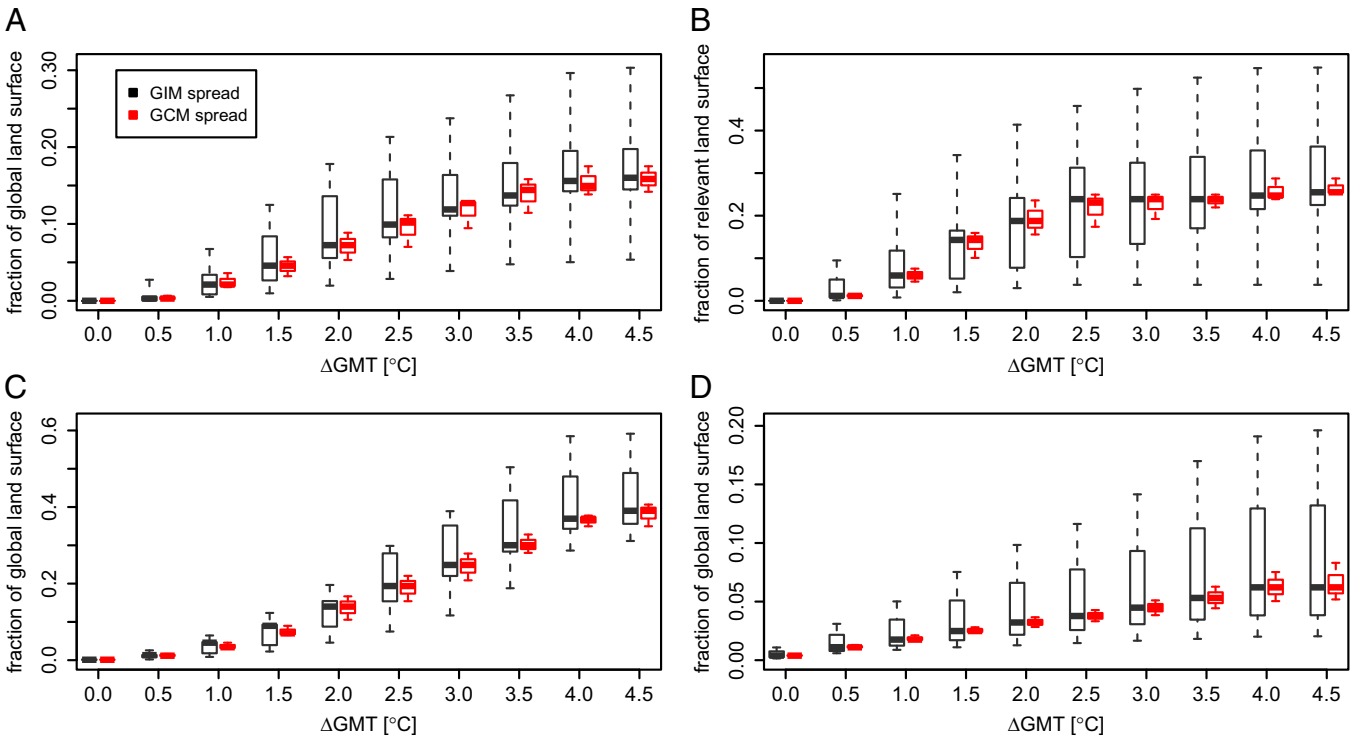

Fig. 3. Cumulative fraction of global land area (excluding Antarctica; for crop yields the relevant area is the maximum crop area as covered today by the four staple crops: maize, wheat, soy, and rice) having crossed the respective sectoral thresholds up to the given ΔGMT for discharge (*A*), crop yields (*B*), risk of severe ecosystem changes (*C*), and LTS (*D*). Black boxes show the uncertainty across impact models, and red boxes indicate the uncertainty across GCMs. Each box indicates the interquartile range, the thick line shows the median, and the whiskers extend over the whole range of the distribution of all GCMs/GIMs at that temperature bin. Note the different ranges on the *y* axis for each panel.

accompanying this study with detailed sectoral understanding and analysis, which can be found elsewhere in this issue (see also *SI Text*) (15, 21, 22).

This high level of uncertainty warrants the strict robustness limit of 50% agreement among GIM-GCM combinations used for the identification of hotspots. At the same time, this uncertainty may mask a remaining risk, given that models appearing at the ends of the distribution cannot be disregarded because no performance-weighting of models was carried out. Therefore, we also provide a worst-case assessment of multisectoral hotspots, with crossing temperatures determined as the 10th percentile of all crossing temperatures in a given grid cell. This process means that only 10% of all GIM-GCM combinations have to agree on the threshold crossing (chosen to have at least two in a sector, to avoid spurious effects of one outlier) and the resulting crossing temperatures are lower limits. This worst-case assessment shows a large additional extent of multisectoral overlap (Fig. 2, dark gray areas) with almost all of the world's inhabited areas affected. The areas with highest exposure in this case have an overlap of all four sectors (Fig. 3 and Fig. S7). This worst case is rather extreme, but nonetheless it represents the upper end of the risk spectrum in light of the large uncertainties.

Aggregate Effects with GMT. The total global area and population that are projected to face average conditions that are considered rare today in more than one sector increases with GMT (Fig. 4).

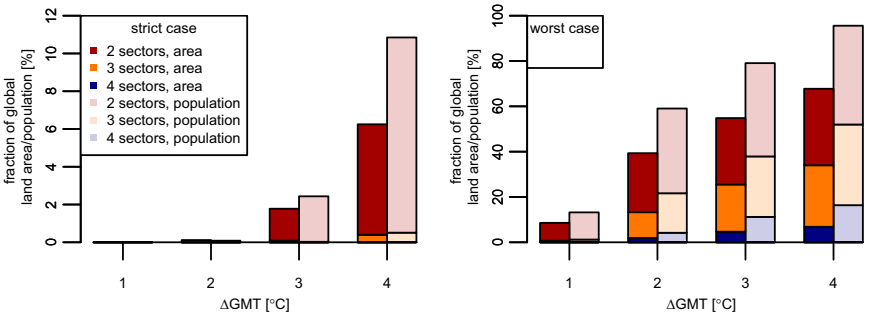

Fig. 4. Cumulative fraction of the global area (brightly tinted bars, excluding Antarctica) and population (lightly tinted bars) affected by the thresholds being crossed at ΔGMT in at least two (red), three (orange), and four (blue) overlapping sectors. (*Left*) The strict case (agreement of at least 50% of GIM-GCM combinations on the threshold crossing). (*Right*) The worst-case (agreement of at least 10% of GIM-GCM combinations on the threshold crossing and the sectoral crossing temperature is the 10th percentile of all crossing temperatures) assessment. Overlap of four sectors does not occur in the strict case. Population is held constant at the year 2000 levels.

The likelihood for multisectoral overlap increases with the area affected in the individual sectors, one reason for the onset of multisectoral pressures at relatively high levels of GMT change only. For the strict assessment, multisectoral severe pressure begins at ΔGMT = 3 °C above the 1980–2010 baseline; at 4 °C roughly 6% of the global area (excluding Antarctica) and close to 11% of the global population are affected. Correspondingly, the largest increases in the areas having crossed the thresholds in each sector are seen between ΔGMT = 1 °C and 3 °C (Fig. 3), with some indications for saturation after that. Further increases in affected areas are possible at higher ΔGMT levels than studied here. For example, a peak and possible later decline in crop yields is expected as a result of heat stress overtaking the initial benefits of the CO_2 fertilization effect.

In the worst-case analysis, area and population affected is already much larger at lower levels of ΔGMT, with the largest increase between 1 °C and 2 °C above the 1980–2010 baseline and an inflection of the trend after that. Almost the entire global population is exposed to multisectoral pressure at ΔGMT = 4 °C. In addition, roughly 18% of the global population is projected to experience severe pressure in all four sectors. The affected regions are in Europe, North America, and south-east Asia (Fig. S7), driven by the extension of malaria prevalence to higher latitudes. This interpretation may give too much emphasis to this pressure, as malaria distribution also depends strongly on socioeconomic factors but is here only driven by climate suitability (26). Nevertheless, the increased overlap of three or even four sectors in the worst-case assessment indicates a strong adaptation pressure, albeit at low probability.

Implications and Further Research

This identification of multisectoral hotspots of climate change impacts is to our knowledge unique in its use of a consistent framework with multiple impact models per sector and using ΔGMT as a metric for climate change. Our global analysis provides a starting point for more detailed understanding of the extended implications of climate change for exposure and adaptation actions. Although geographically overlapping impacts only start at ΔGMT = 3 °C above the 1980–2010 baseline (almost 4 °C above preindustrial GMT levels), large increases in exposed areas within the sectors start at around 2.2 °C above preindustrial levels. In the worst-case analysis, the largest increase in affected area and population occurs between roughly 2 °C and 3 °C above preindustrial levels. This finding provides important insight for mitigation strategies.

The identified multisectoral hotspots are geographically diverse, including the southern Amazon basin, southern Europe, the Ethiopian highlands, and northern India, and are driven by different combinations of coinciding sectors. Implications and possible feedbacks between the overlapping sectors can be investigated in regional case studies. At the same time, these hotspots could affect distant regions through indirect effects, such as trade or migration. Appropriate adaptation planning that considers coinciding (and also interacting) pressures facilitates the development of strategies designed to address such multiple challenges, and avoids creating solutions for one pressure that possibly seriously exacerbates another (e.g., draining wetlands to reduce malaria in an area prone to increases in flooding).

The set-up for our analysis explicitly includes uncertainty in both climate and impact models. This format shows that uncertainties from both GIMs and GCMs are large, limiting the robustness of the conclusions; however, it should not hamper action at this point, as some level of uncertainty will always be present. In particular the low probability-high impact worst-case assessment, which shows a very large extent of multisectoral pressures starting at lower temperature changes, provides a strong motivation for more detailed impacts research.

Because it is unique, our analysis is a methodological experiment, to be refined in the light of experience. Indeed, different patterns may emerge if different sectors or absolute magnitudes of change are included. A comparison of hotspots generated with different methodologies will provide valuable insights into impact dynamics. The identification of hotspots of positive climate-change impacts would create a more balanced and comprehensive picture, but requires different metrics to those used here. In addition, although a simple overlap of the different sectoral metrics is considered here, the challenge for future analyses is also to integrate the interactions between the different sectors and indirect effects over large distances, which may alter the spatial pattern of hotspots. Examples are interactions between water availability and irrigation or ecosystem services, and irrigation and malaria occurrence (27). Furthermore, a more comprehensive understanding of human vulnerability hotspots requires a thorough analysis, combining highly resolved indicators of adaptive capacity and sensitivity (which so far seem to be lacking) with biophysical hotspot indicators as measures of exposure (2, 3). Nevertheless, our study is an important step toward a consistent integration of multiple sectors in impacts research, and identifies the risk of sizable hotspots of multisectoral pressures under highly plausible levels of global warming.

Materials and Methods

Models and Data. For this analysis, simulations were driven by the three ISI-MIP GCMs that exhibit a ΔGMT= 4 °C by the end of the 21st century (HadGEM2-ES, MIROC-ESM-CHEM, IPSL-CM5A-LR). To improve statistical agreement with observations, a bias correction was applied to the climate data. This bias constitutes an additional source of uncertainty and reduces the spread of present-day GCM climatologies (28–31). The gridded year 2000 population data are based on United Nations World Populations Prospects data, scaled to match the country totals of the new Shared Socio-Economic Pathway population projections for the middle-of-the-road case (SSP2; https://secure.iiasa.ac.at/web-apps/ene/SspDb) using the National Aeronautics and Space Administration GPWv3 y-2010 (http://sedac.ciesin.columbia.edu/data/collection/gpw-v3) gridded population dataset (32, 33). Similar results for the percentage of affected global population are found when the projected values for 2084 are used (Fig. S8). Impacts were simulated on terrestrial pixels of a global 0.5° mesh (roughly 55 km wide at the equator). For an overview of the GIMs used in the analysis, see Tables S1–S4, accompanied by a brief discussion of model differences contributing to the spread in results. The global gridded crop model intercomparison was coordinated by the Agricultural Model Intercomparsion and Improvement Project (34).

Impact Metrics. All metrics have annual temporal resolution, neglecting seasonal patterns. To avoid spurious effects, values are set to zero below the lower limits 0.01 $km^3 \cdot yr^{-1}$ and 2.5% natural vegetation cover, for discharge and ecosystem change, respectively (15, 35). The four crops are combined by converting to energy-weighted production per cell using the following conversion factors for energy content (MJ kg^{-1} dry matter): wheat (spring/winter), 15.88; rice (paddy), 13.47; maize, 16.93; soy, 15.4 (36, 37). The extent of potential agricultural hotspots is limited; for example, millet and sorghum, which are widely grown in Africa, are not included in the analysis. The impact of climate change on malaria occurrence focuses on changes in LTS. This simple metric represents an aggregated risk factor because it neglects age-dependent immunity acquisition associated with transmission intensity. Increases in impacts associated with transitions from malaria-free to epidemic conditions are also not considered.

Hotspots Method. GMT is calculated from the GCM data and change is measured with respect to the reference period 1980–2010. The GMT level in the reference period is ~0.7 °C above preindustrial, based on estimates for 1980–1999 of 0.51 °C and the average of the five GCMs in ISI-MIP (20). Simulations are binned in temperature bins at ΔGMT = 1 °C, 2 °C, 3 °C, and 4 °C (±0.5 °C). For GIM-GCM combinations where the threshold has not been crossed by ΔGMT = 4.5 °C (the highest temperature bin achieved by GCMs in this study), a value of 5 is assigned. Consequently, cells with a median sectoral crossing temperature above 4.5 °C are not included in the analysis, effectively excluding cells with less than 50% agreement of GIM-GCM combinations on the crossing of the respective threshold. See *SI Text* for

more details on the sensitivities and uncertainties of the method. If a grid cell is identified as having crossed the threshold, the whole area of the grid-cell is assumed to be affected. This process neglects, for example, the separation of agricultural and natural vegetation areas in a grid-cell, which is below the resolution of the analysis. The spread across GIMs is calculated by taking the median over all GCMs for each GIM. The corresponding procedure is used for GCMs.

ACKNOWLEDGMENTS. We thank the anonymous referees for detailed and valuable comments greatly improving this paper; the World Climate Research Programme's Working Group on Coupled Modelling, which is responsible for Coupled Model Intercomparison Project; and the climate modeling groups for producing and making available their model output. The Inter-sectoral Impact Model Intercomparison Project Fast Track project underlying the framework of this paper was funded by the German Federal Ministry of Education and Research (01LS1201A). For the Coupled Model Intercomparison Project, the US Department of Energy's Program for Climate Model Diagnosis and Intercomparison provides coordinating support and led development of software infrastructure in partnership with the Global Organization for Earth System Science Portals. This study was funded in part by the European Framework Programme FP7/20072013 under Grants 266992 (to F.P.) and 238366 (to A.F.); Joint Department of Energy and Climate Change/Defra Met Office Hadley Centre Climate Programme GA01101 (to D.H.); the Federal Ministry for the Environment (K.F.); the Nature Conservation and Nuclear Safety 11_II_093_Global_A_SIDS_and_LDCs (to K.F.); EUFP7 Quantifying Weather and Climate Impacts on Health in Developing Countries (QWeCI) and HEALTHY FUTURES projects (F.d.J.C.G.); and the Environment Research and Technology Development Fund (S-10) of the Ministry of the Environment, Japan (to Y.M. and K. Nishina). T.A.M.P. acknowledges support from EU FP7 project EMBRACE (Earth System Model Bias Reduction and Assessing Abrupt Climate Change) (Grant 282672).

1. Warren R (2011) The role of interactions in a world implementing adaptation and mitigation solutions to climate change. *Phil Trans R Soc A Math Phys Eng Sci* 369(1934): 217–241.
2. Yohe G, et al. (2006) Global distributions of vulnerability to climate change. *The Integrated Assessment Journal* 6(3):35–44.
3. Fraser EDG, Simelton E, Termansen M, Gosling SN, South A (2013) "Vulnerability hotspots": Integrating socio-economic and hydrological models to identify where cereal production may decline in the future due to climate change induced drought. *Agric For Meteorol* 170:195–205.
4. Giorgi F (2006) Climate change hot-spots. *Geophys Res Lett* 33(8):L08707.
5. Baettig MB, et al. (2007) A climate change index: Where climate change may be most prominent in the 21st century. *Geophys Res Lett* 34(1):L01705.
6. Diffenbaugh NS, Giorgi F (2012) Climate change hotspots in the CMIP5 global climate model ensemble. *Clim Change* 114(3-4):813–822.
7. Patz JA, Kovats RS (2002) Hotspots in climate change and human health. *BMJ* 325(7372):1094–1098.
8. Warszawski L, et al. (2014) The Inter-Sectoral Impact Model Intercomparison Project (ISI–MIP): Project framework. *Proc Natl Acad Sci USA* 111:3228–3232.
9. Meinshausen M, et al. (2009) Greenhouse-gas emission targets for limiting global warming to 2 °C. *Nature* 458(7242):1158–1162.
10. UNFCCC (2009) Report of the Conference of the Parties on its Fifteenth session, and Addendum Part Two: Decisions adopted by the Conference of the parties. Copenhagen, Denmark, December 7–19, 2009.
11. Sachs J, Malaney P (2002) The economic and social burden of malaria. *Nature* 415(6872):680–685.
12. Portmann FT, Siebert S, Döll P (2010) MIRCA2000-global monthly irrigated and rainfed crop areas around the year 2000: A new high-resolution data set for agricultural and hydrological modeling. *Global Biogeochem Cycles* 24(1):GB1011.
13. Heyder U, Schaphoff S, Gerten D, Lucht W (2011) Risk of severe climate change impact on the terrestrial biosphere. *Environ Res Lett*, 10.1088/1748-9326/6/3/034036.
14. Mortimore M (2010) Adapting to drought in the Sahel: Lessons for climate change. *WIREs Clim Change* 1(1):134–143.
15. Warszawski L, et al. (2013) A multi-model analysis of risk of ecosystem shifts under climate change. *Environmental Research Letters* 8:044018.
16. Folke C, et al. (2004) Regime shifts, resilience, and biodiversity in ecosystem management. *Annu Rev Ecol Evol Syst* 35:557–581.
17. Kumar P (2010) *The Economics of Ecosystems and Biodiversity: Ecological and Economic Foundations* (Earthscan, London, Washington).
18. Van Vuuren DP, et al. (2011) The representative concentration pathways: An overview. *Clim Change* 109:5–31.
19. Peters GP, et al. (2013) The challenge to keep global warming below 2 °C. *Nature Climate Change* 3(3):4–6.
20. Brohan P, Kennedy J, Harris I, Tett S, Jones P (2006) Uncertainty estimates in regional and observed temperature changes: A new data set from 1850. *J Geophys Res-Atmos* 111(D12):106–127.
21. Schewe J, et al. (2014) Multi-model assessment of water scarcity under climate change. *Proc Natl Acad Sci USA* 111:3245–3250.
22. Rosenzweig C, et al. (2014) Assessing agricultural risks of climate change in the 21st century: A global gridded crop model intercomparison. *Proc Natl Acad Sci USA* 111:3268–3273.
23. Chaves LF, Koenraadt CJM (2010) Climate change and highland malaria: Fresh air for a hot debate. *Q Rev Biol* 85(1):27–55.
24. Hirabayashi Y, Kanae S, Emori S, Oki T, Kimoto M (2008) Global projections of changing risks of floods and droughts in a changing climate. *Hydrol Sci J* 53(4): 754–772.
25. Hagemann S, et al. (2013) Climate change impact on available water resources obtained using multiple global climate and hydrology models. *Earth Syst Dynam.* 4(1): 129–144.
26. Béguin A, et al. (2011) The opposing effects of climate change and socio-economic development on the global distribution of malaria. *Glob Environ Change* 21(4): 1209–1214.
27. Elliott J, et al. (2014) Constraints and potentials of future irrigation water availability on agricultural production under climate change. *Proc Natl Acad Sci USA* 111: 3239–3244.
28. Chen C, Haerter JO, Hagemann S, Piani C (2011) On the contribution of statistical bias correction to the uncertainty in the projected hydrological cycle. *Geophys Res Lett* 38(20):L20403.
29. Hempel S, Frieler K, Warszawski L, Schewe J, Piontek F (2013) A trend-preserving bias correction—The ISI-MIP approach. *Earth Syst Dynam Discuss* 4:49–92.
30. Hagemann S, et al. (2011) Impact of a statistical bias correction on the projected hydrological changes obtained from three GCMs and two hydrological models. *J Hydrometeorol* 12(4):556–578.
31. Ehret U, Zehe E, Wulfmeyer V, Warrach-Sagi K, Liebert J (2012) Should we apply bias correction to global and regional climate model data? *Hydrol Earth Syst Sci Discuss* 9: 5355–5387.
32. van Vuuren DP, et al. (2012) A proposal for a new scenario framework to support research and assessment in different climate research communities. *Glob Environ Change* 22(1):21–35.
33. UNDESA (2010) *World Population Prospects, the 2010 Revision* (UNDESA, New York).
34. Rosenzweig C, et al. (2012) The Agricultural Model Intercomparison and Improvement Project (AgMIP): Protocols and pilot studies. *Agric For Meteorol*, 170:166–182.
35. Von Bloh W, Rost S, Gerten D (2010) Efficient parallelization of a dynamic global vegetation model with river routing. *Environmental Modeling* 25(6):685–690.
36. Wirsenius S (2000) *Human Use of Land and Organic Materials* (Chalmers Univ of Technology and Göteborg University, Gothenburg, Sweden).
37. FAO (2001) *Food Balance Sheets: A Handbook* (FAO, Rome).

Supporting Information

Piontek et al. 10.1073/pnas.1222471110

Characteristics of the Global Impact Models

Model Overview. Tables S1–S4 give an overview of the main characteristics of the global impact models (GIMs) used in this analysis. For more detailed descriptions and comparisons, see the sectoral reports by Rosenzweig et al. (1), Schewe et al. (2) and, Warszawski et al. (3).

Important Characteristics of Impact Models and Model Uncertainty. For each sector, the set of impact models is rather diverse, leading to a large spread of results. Here a few of the key responsible features are discussed.

The crop model ensemble consists of models covering a broad range of management assumptions (e.g., static vs. adaptive management, nutrient-limited vs. nonlimited systems), effectively reflecting different degrees of autonomous adaptation. In this analysis, focusing on negative effects (i.e., decreases in crop yields) models with adaptive management provide a lower limit for regions affected by crossing the threshold. The effect of CO_2 fertilization is of great importance for crop models, biomes models, and to a limited degree hydrological models (not all hydrological models include it), but still subject to high uncertainty (4, 5). Here, full CO_2 fertilization is assumed as represented in the respective models, as an analysis of the influence of this effect is beyond the scope of this report. For crop models, this adds a further uncertainty because nitrogen fertilization has not been standardized among the models but can possibly reduce the CO_2 effect, leading to optimistic crop yields projections. For further details, see Rosenzweig et al. (1).

The main factors of uncertainty for global hydrological models result from applying different snow schemes, as well as approaches to calculating potential evapotranspiration (6). Other sources are soil parameters and vegetation cover, as well as the rainfall-runoff response. For this analysis, the models are used only in setups without human influence. For further details, see Schewe et al. (2).

Of the four global malaria models included, only one is a dynamic model running with a daily integration time step (VECTRI). This model also explicitly attempts to model the impact of climate on the vector and parasite life cycles. The other three models use statistical relationships based on monthly climate data. The models also differ in their parameterizations in terms of species of malaria parasites, restricting transmission in some models (MARA, LMM) to the tropics and subtropics; others also cover higher latitudes (VECTRI, MIASMA). The former are better suited to study present day malaria distributions, while the latter better represent distributions without human interventions aiming at eradicating malaria. This process results in very limited agreement among models, both for present day and future distribution of malaria. For more discussion on advantages and disadvantages of different modeling types see Rogers and Randolph (7).

Biomes models mainly fall into two categories: those that include dynamic vegetation and those that do not. Other differences include the modeling of permafrost, fire, and the nitrogen cycle. Two of the seven biomes models provided results on a coarser resolution. For further details, see Warszawski et al. (3).

Characteristics of the Sectoral Metrics

The metrics used here capture only a subset of effects relevant to the livelihoods of people and clearly, socioeconomic conditions, livelihood strategies, and specific climate-change adaptation will have a large influence on the vulnerability of societies to these four areas of change. Adaptation options, as well as other relevant characteristics for each sectoral metric, are briefly discussed below.

Changes in discharge as a measure of water availability affect daily life, as well as industrial production, energy supply, and especially agriculture. However, temporal variability (floods and droughts), as well as spatial distribution in river basins, are possibly of even greater importance. Both could be managed to some extent through efficient integrated water resource management (8).

The four crops used in this analysis do not cover the full breadth of effects in agriculture, although they are among the most commonly traded agricultural commodities. Furthermore, the analysis is limited to regions where these crops are currently cultivated, which limits regions of possible multisectoral overlap (Fig. S1). Because only negative changes are considered, a possible expansion of cropland to higher latitudes, which is not accounted for because of the masking, is not important. Furthermore, drops in crop yields could be managed by a variety of measures, including shifts in crop types, more productive cultivars, or optimizing fertilization or irrigation, options that are not taken into account here (9, 10).

The threshold for both discharge and crop yields was chosen to be the 10th percentile of the present day distribution in a given grid cell. Although this choice signifies a moderately extreme shift of average conditions, it is not a shift to very extreme conditions, like droughts. To test the sensitivity of the method to this threshold, we repeated the analysis for a fifth percentile threshold (a 16-y return period). Although the total area experiencing a threshold crossing is smaller, the pattern of increase with respect to global mean temperature (GMT) is robust (Fig. S2).

The Γ-metric assumes changes in the biogeochemical state of vegetated land surface to be a proxy for the risk of ecosystem shifts. This includes the components change in vegetation structure, relative changes to carbon and water fluxes, relative changes in carbon and water fluxes and absolute changes and fluxes in carbon and water stocks. Not all biomes models provide all variables necessary for the metric, which were then left out of the calculation. For models without dynamic vegetation composition the other components of the metric were scaled up accordingly. The changes in the metric dimensions (running means compared to the baseline period) are aggregated into the Γ-metric as one normalized measure following Heyder et al. (11), all with equal weighting after being normalized to a value between 0 and 1. The metric covers the range 0 to 1, where $\Gamma = 0$ means no change of vegetation states, while an extensive change from one biome to a completely different one would mean a Γ of very close to 1. Simultaneous change in multiple components results in an increased risk of ecosystem shift compared to individual changes. The level of $\Gamma > 0.3$ defined as threshold for risk of severe ecosystem change corresponds, for an illustration, for example to a change between a warm wood- and shrubland and a tropical seasonal forest, based on the LPJmL model (11). Adaptation to ecosystem changes is of course possible, but adaptation measures depend strongly on the region and societal needs. Finally, malaria is only one example of health impacts of climate change with particular relevance for tropical countries. Malaria was eradicated in Europe and the United States only in the first half of the last century through a combination of farming measures, better living conditions, and medical care, and the extension of climate conditions favorable for malaria toward higher latitudes does not necessarily indicate existence of pathogens or large-scale outbreaks of malaria there. The inclusion of malaria strongly limits opportunities for multisectoral overlap,

because most regions where malaria is prevalent today already have a transmission season larger than the sectoral threshold of 3 mo (Fig. S3). A crossing of this threshold can only happen in fringe areas, higher altitudes, or higher latitudes. Because only two of the four models consider spread to higher latitudes, this leads to the very small total area robustly sensitive to this metric. This result mirrors the limited importance climate change is expected to have on global malaria prevalence [see also, for example, Lafferty (12)].

Supporting Figures

Sectoral Threshold Crossings. Fig. S4 shows a larger version of Fig. 1, to help distinguish individual sectoral features.

Uncertainty. This section illustrates the discussion on uncertainty with supporting figures, relating to multisectoral hotspot patterns based on individual global climate models (GCMs) (Fig. S5), uncertainty of crossing temperatures (Fig. S6), and sectoral as well as multisectoral hotspots patterns for the worst-case assessment (Fig. S7).

Population Growth

The affected population is calculated assuming constant population based on the year 2000, which avoids an entanglement of effects of population growth and increasing global warming. However, population is expected to growth strongly over the century. In the Shared Socio-Economic Pathway (SSP2) population scenario (https://secure.iiasa.ac.at/web-apps/ene/SspDb) used as baseline in the Intersectoral Impact Model Intercomparison Project (ISI-MIP), an increase from 6 billion people in 2000 to 9.9 billion people in 2084 is projected, a factor of 1.64. The highest increase in population density is projected for regions already dense, such as India, as well as for Sub-Saharan Africa. As the areas of high population density do not shift much, the population increase does not have a strong effect on the fraction of global population projected to be affected by multisectoral pressure (Fig. S8).

Overview of the GCMs Considered in the Analysis

In this analysis three GCMs are considered:

The model from the Met Office Hadley Centre, with additional HadGEM2-ES realizations contributed by Instituto Nacional de Pesquisas Espaciais. The model version used is HadGEM2-ES.

The model from Institut Pierre-Simon Laplace (IPSL), model version IPSL-CM5A-LR.

The MIROC model of the Japan Agency for Marine-Earth Science and Technology, the Atmosphere and Ocean Research Institute at the University of Tokyo, and the National Institute for Environmental Studies, model version MIROC-ESM-CHEM.

1. Rosenzweig C, et al. (2013) Assessing agricultural risks of climate change in the 21st century: A global gridded crop model intercomparison. *Proc Natl Acad Sci USA*, 10.1073/pnas.1222463110.
2. Schewe J, et al. (2013) Multimodel assessment of water scarcity under climate change. *Proc Natl Acad Sci USA*, 10.1073/pnas.1222460110.
3. Warszawski L, et al. (2013) A multi-model analysis of risk of ecosystem shifts under climate change. *Environmental Research Letters* 8:044018.
4. Long SP, Ainsworth EA, Leakey ADB, Nösberger J, Ort DR (2006) Food for thought: Lower-than-expected crop yield stimulation with rising CO_2 concentrations. *Science* 312(5782):1918–1921.
5. Tubiello FN, et al. (2007) Crop response to elevated CO2 and world food supply: A comment on "Food for Thought. . ." by Long et al., *Science* 312:1918–1921, 2006. *Eur J Agron* 26(3):215–223.
6. Haddeland I, et al. (2011) Multimodel estimate of the global terrestrial water balance: Setup and first results. *J Hydrometeorol* 12(5):869–884.
7. Rogers DJ, Randolph SE (2000) The global spread of malaria in a future, warmer world. *Science* 289(5485):1763–1766.
8. Pahl-Wostl C, Kabat P, Möltgen J (2008) *Adaptive and Integrated Water Management* (Springer, Heidelberg, Berlin).
9. Howden SM, et al. (2007) Adapting agriculture to climate change. *Proc Natl Acad Sci USA* 104(50):19691–19696.
10. Mueller ND, et al. (2012) Closing yield gaps through nutrient and water management. *Nature* 490(7419):254–257.
11. Heyder U, Schaphoff S, Gerten D, Lucht W (2011) Risk of severe climate change impact on the terrestrial biosphere. *Environ Res Lett*, 10.1088/1748-9326/6/3/034036.
12. Lafferty KD (2009) The ecology of climate change and infectious diseases. *Ecology* 90(4):888–900.

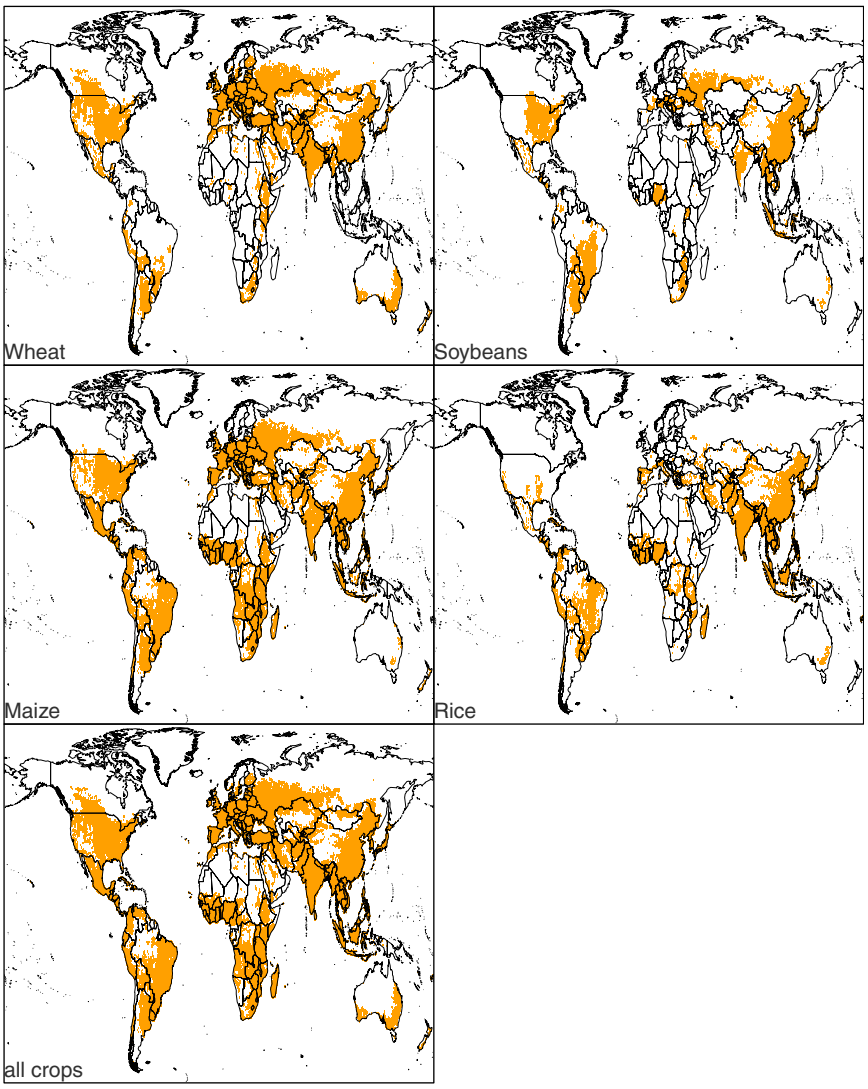

Fig. S1. Present-day mask for areas growing the four crops considered on currently rain-fed and irrigated cropland (1). The combined map shows the total resulting area relevant for hotspot analysis of crop yields in this analysis. This limits the area where all four metrics can cross the present-day thresholds.

1. Portmann FT, Siebert S, Döll P (2010) MIRCA2000-global monthly irrigated and rainfed crop areas around the year 2000: A new high-resolution data set for agricultural and hydrological modeling. *Global Biogeochem Cycles* 24(1):GB1011.

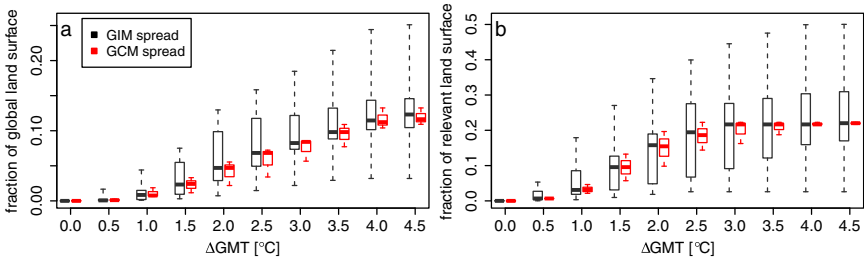

Fig. S2. Test applying a stricter threshold to be crossed for discharge (*A*) and crop yields (*B*); instead of the 10th percentile the 5th percentile is used. The cumulative fraction of global relevant land area having crossed this threshold is shown. Black boxes show the uncertainty among impact models, and red boxes indicate the uncertainty among GCMs. Each box indicates the interquartile range and the median (thick line). The whiskers show the whole range of the distribution of all GIM-GCM combinations at that temperature bin.

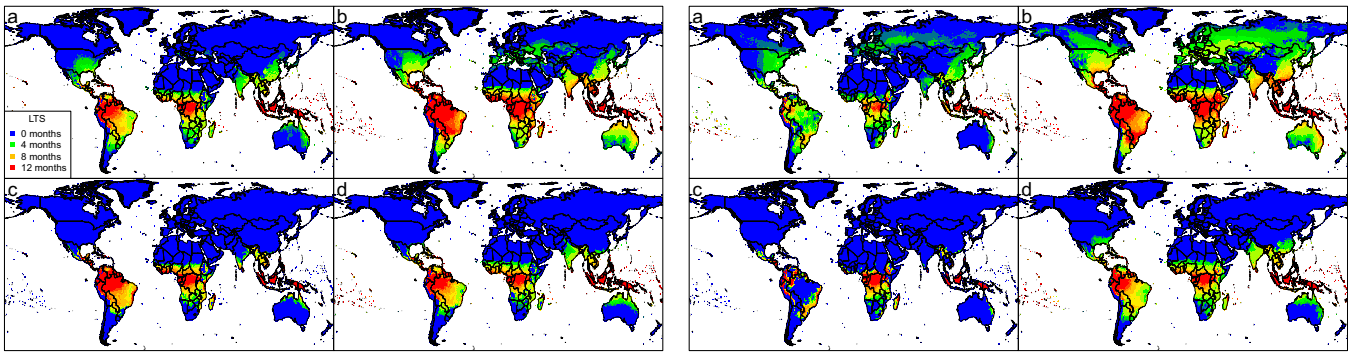

Fig. S3. Length of transmission season in months for the four malaria models: Liverpool Malaria Model (LMM) (*A*), Modeling Framework for the Health Impact Assessment of Man-Induced Atmospheric Changes (MIASMA) (*B*), vector-borne disease community model of the International Centre for Theoretical Physics, Trieste (VECTRI) (*C*), and Mapping Malaria Risk in Africa (MARA) (*D*). Median over the three GCMs for representative concentration pathways (RCP8.5) for the reference period (1980–2010, *Left A–D*) and the end of the century (2069–2099, *Right A–D*).

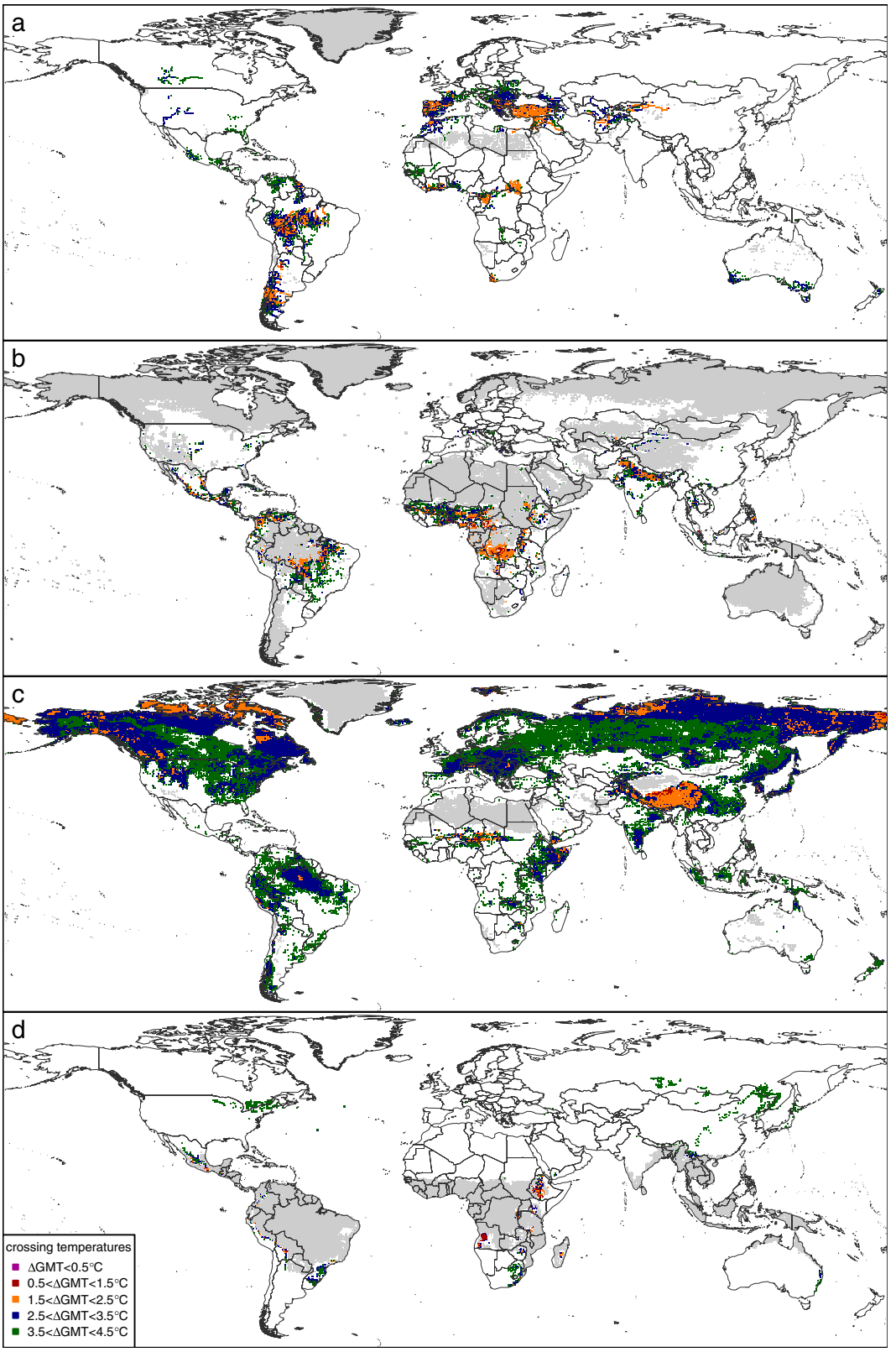

Fig. S4. Threshold crossing temperatures with respect to the reference period GMT for the four sectoral metrics: discharge (*A*), crop yields (*B*), risk of severe ecosystem change (*C*), and length of transmission season of malaria (*D*). Areas in white do not cross the respective threshold. The gray color indicates regions which are either masked out [discharge, Γ, crop yields (only regions where maize, what, soy, and rice are currently cultivated are considered)], or where malaria is already endemic (*D*). An agreement of 50% of all GIM-GCM combinations on threshold crossing is required for consideration in the analysis.

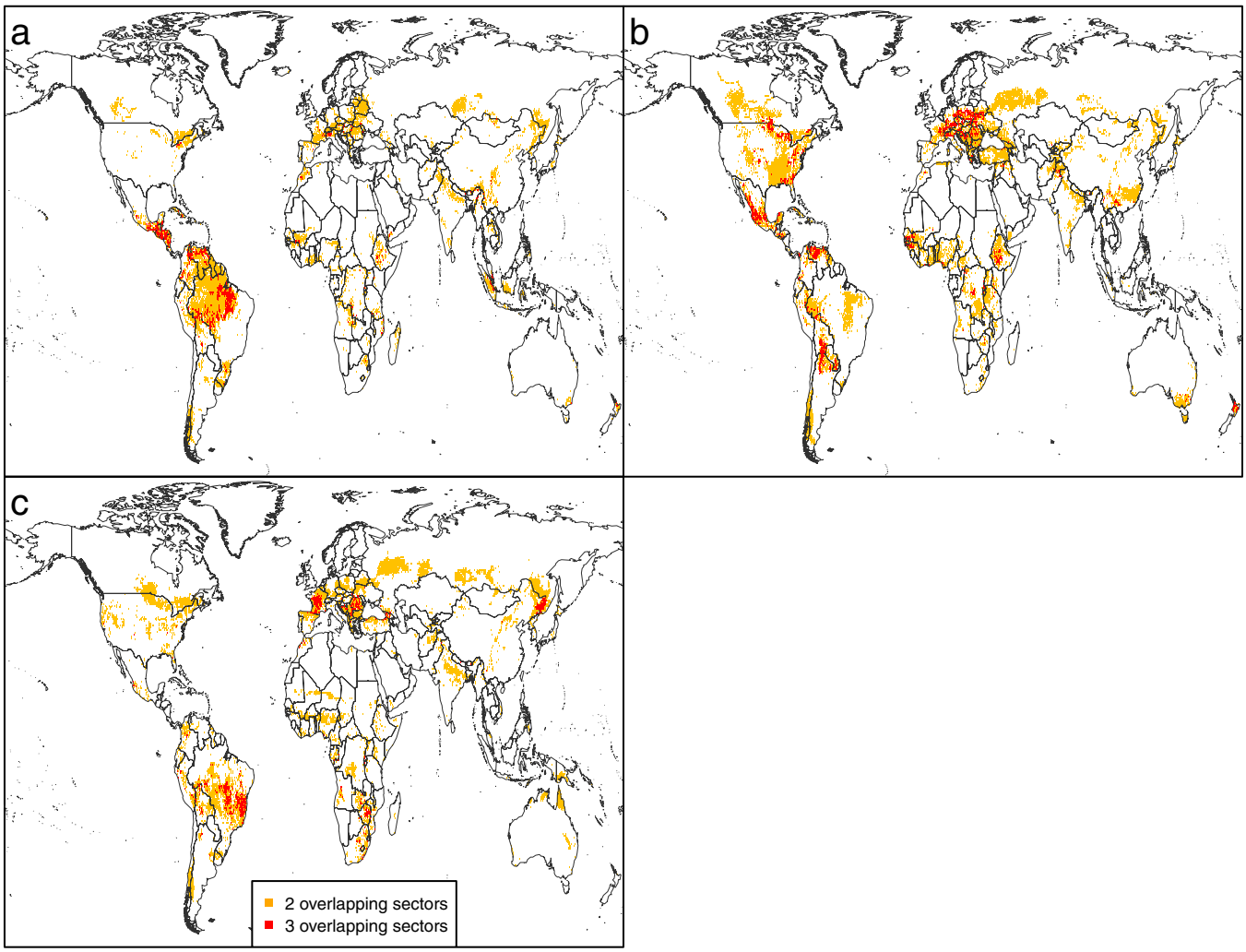

Fig. S5. Multisectoral hotspots of impacts for two (orange) and three (red) overlapping sectors, calculated separately for the three GCMs HadGEM2-ES (*A*), IPSL-CM5A-LR (*B*), and MIROC-ESM-CHEM (*C*), in the strict assessment, with 50% of respective GIM-GCM combinations agreeing on the threshold crossing in each sector. The emerging hotspot patterns are very different, especially in South America and the eastern United States, yet there is some consistency in the results for Europe, Central America, and Africa. This finding underlines the effects of GCM uncertainty on the possible hotspots as discussed in the *The Role of Uncertainty* in the main text. A similar plot for individual GIMs cannot be shown because they are different in each sector.

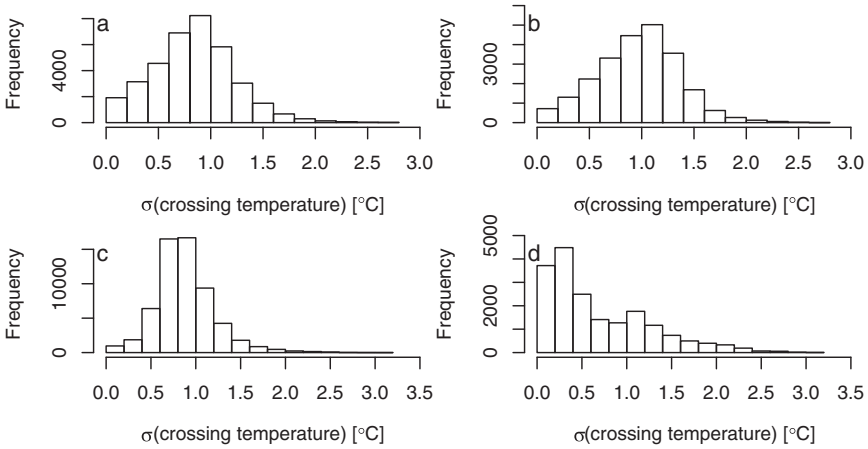

Fig. S6. SD of crossing temperatures taken over those GIM-GCM combinations that do cross for discharge (*A*), crop yields (*B*), risk of severe ecosystem changes (*C*), and length of malaria transmission season (*D*).

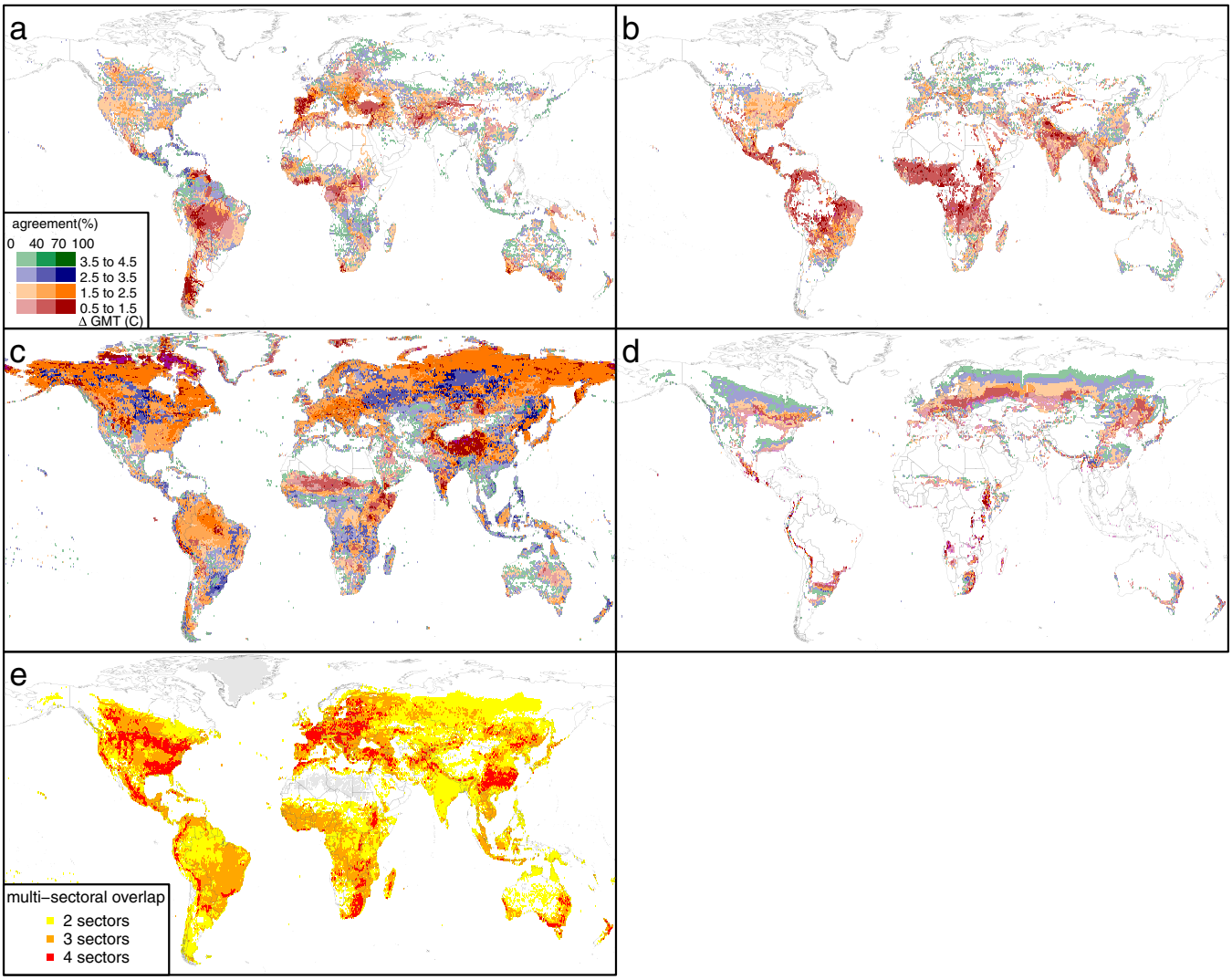

Fig. S7. Sectoral distribution of worst-case analysis of threshold crossings (*A–D*) and multisectoral overlap colored by number of overlapping sectors (*E*). The sectoral crossing temperature is taken as the 10th percentile of all GIM-GCM crossing temperatures, requiring an agreement of 10% on the crossing, to avoid spurious results of one model only. The different color shadings represent agreement of impact models on the crossing of the threshold. This visualization style is based on Kaye et al. (1). The multisectoral overlap is for the range of ΔGMT up to 4.5 °C. The light gray colored areas in *E* are regions where no overlap is possible at all because of masking.

1. Kaye NR, Hartley A, Hemming D (2012) Mapping the climate: Guidance on appropriate techniques to map climate variables and their uncertainty. *Geosci Model Dev* 5(1):245–256.

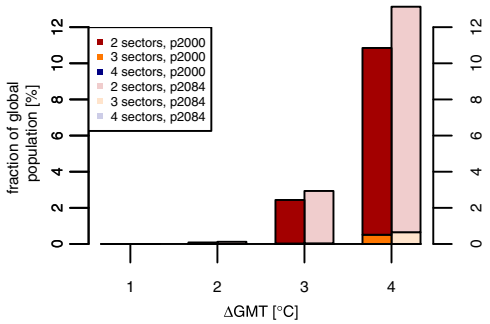

Fig. S8. Comparing the cumulative fraction of global population affected by multisectoral pressure under the strict assumptions when based on the year 2000 distribution (brightly tinted bars) and when based on the year 2084 distribution (lightly tinted bars).

Table S1. Overview and main characteristics of global crop models

Model name	CO_2 fertilization affects	Nutrient constraints on CO_2 fertilization	Fertilizer use	Adaptation measures	Starting conditions (representation of present day yields or potential yields?)
EPIC (1, 2) Environmental Policy Integrated Climate	RUE, TE	No	Flexible N application rates (N stress free days in 90% of crop growing period to an upper application limit of 200 kg·ha^{-1}) Constant P application rates.	Annual adjustment of planting dates; total heat units to reach maturity remain constant no adjustment of cultivars	Present day potential yields
GEPIC (3, 4) GIS-based agroecosystem model integrating a bio-physical EPIC model (Environmental Policy Integrated Climate) with a GIS	RUE, TE	No	Flexible N application based on N stress >10% (limitation of potential biomass increase because of N stress) up to an upper national application limit according to FertiStat, fixed present day P application rates following FAO FertiStat database*	Decadal adjustment of planting dates, total heat units to reach maturity remain constant. Adjustment of winter and spring wheat sowing areas based on temperature	Present day yields
GAEZ-IMAGE (5, 6) Integrated Model to Assess the Global Environment	LLP	No	Soil nutrient limiting factors are not accounted for	Adjustment of planting dates, total heat units to reach maturity remain constant. Adjustment of summer and winter varieties in case of wheat and maize	Present day yields
LPJ-GUESS (7) – Lund-Potsdam-Jena General Ecosystem Simulator with managed Land	LLP, CC	No	Soil nutrient limiting factors are not accounted for	Adjustment of planting dates, total heat units to reach maturity are dynamically adapted to the prevailing climate	Potential yields
LPJmL (8, 9) - Lund-Potsdam-Jena managed Land Dynamic Global Vegetation and Water Balance Model	LLP, CC	Not directly accounted for	Soil nutrient limiting factors are not accounted for	Fixed planting dates, total heat units to reach maturity remain constant	Present day yields
PEGASUS (10) Predicting Ecosystem Goods And Services Using Scenarios	RUE, TE	No	Fixed N, P, K application rates (IFA national statistics)	Adjustment of planting dates, variable heat units to reach maturity	Present day yields
pDSSAT [11, for DSSAT] – parallel Decision Support System for Agro-technology Transfer	RUE, LLP, CC	Yes for wheat, rice, maize; no for soy	Fixed N present day application rates	No adjustment of planting dates, total heat units to reach maturity remain constant	Present day yields

CC, canopy conductance; GIS, geographic Information system; K, potassium; IFA, International Fertilizer Industry Association; LLP, leaf level photosynthesis; N, nitrogen; P, phosphorus; RUE, radiation use efficiency; TE, transpiration efficiency.
*FAO FertiSTAT: Fertilizer use statistics. Available at: http://www.fao.org/ag/agl/fertistat/index_en.htm.

1. Williams JR (1995) The EPIC Model. *Computer Models of Watershed Hydrology*, ed Singh VP (Water Resources Publications, Highlands Ranch, CO), pp 909–1000.
2. Izaurralde RC, Williams JR, McGill WB, Rosenberg NJ, Jakas MCQ (2006) Simulating soil C dynamics with EPIC: Model description and testing against long-term data. *Ecol Modell* 192(3-4):362–384.
3. Williams JR, Jones CA, Kiniry JR, Spanel DA (1989) The EPIC crop growth model. *Trans ASAE* 32:497–511.
4. Liu JG, Zehnder AJB, Yang H (2009) Global crop water use and virtual water trade: the importance of green water. *Water Resour Res* 45:W05428.
5. MNP (2006) (Eds A.F.Bowman, T. Kram, and K. Klein Goldewijk), *Integrated modelling of global environmental change.* An overview of IMAGE 2.4. Netherlands Environmental Assessment Agency (MNP), Bilthoven, The Netherlands.

6. Leemans R, Solomon AM (1993) Modeling the potential change in yield and distribution of the earth's crops under a warmed climate. *Clim Res* 3(1-2):79–96.
7. Lindeskog M, et al. (2013) Implications of accounting for land use in simulations of ecosystem services and carbon cycling in Africa. *Earth Syst Dynam Discuss* 4:235–278.
8. Bondeau A, et al. (2007) Modelling the role of agriculture for the 20th century global terrestrial carbon balance. *Glob Change Biol* 13(3):679–706.
9. Waha K, et al. (2012) Climate-driven simulation of global crop sowing dates. *Glob Ecol Biogeogr* 21(2):247–259.
10. Deryng D, Sacks WJ, Barford CC, Ramankutty N (2011) Simulating the effects of climate and agricultural management practices on global crop yield. *Global Biogeochem Cycles* 25(2): GB2006.
11. Jones JW, et al. (2003) The DSSAT cropping system model. *Eur J Agron* 18(3-4):235–265.

Table S2. Overview and main characteristics of global hydrological models

Model name	Energy balance	Evaporation scheme	Runoff scheme	Snow scheme	CO_2 effect
DBH (1, 2) – Distributed Biosphere-Hydrological Model	Yes	Energy balance	Infiltration excess	Energy balance	Constant
H08 (3, 4)	Yes	Bulk formula*	Saturation excess, nonlinear	Energy balance	No
JULES (5, 6) - Joint UK Land Environment Simulator	Yes	Penman-Monteith	Infiltration excess, saturation excess, groundwater	Energy balance	Yes
LPJmL (7, 8) - Lund-Potsdam-Jena managed Land Dynamic Global Vegetation and Water Balance Model	No	Priestley-Taylor	Saturation excess	Degree day	Yes
Mac-PDM.09 (9, 10) – Macroscale Probability Distributed Moisture model.09	No	Penman-Monteith	Saturation excess, nonlinear	Degree day	No
MATSIRO (11, 12) – Minimal Advanced Treatments of Surface Interaction and RunOff	Yes	Bulk formula	Infiltration excess, saturation excess, groundwater.	Energy balance	Constant
MPI-HM (13, 14) – Max Planck Institute Hydrology Model	No	Penman-Monteith	Saturation excess, nonlinear	Degree day	No
PCR-GLOBWB (15, 16) – PCRaster Global Water Balance	No	Hamon	Saturation excess β-function†	Degree day	No
VIC (17, 18) – Variable Infiltration Capacity Macroscale Hydrologic Model	Only for snow	Penman-Monteith	Saturation excess, nonlinear	Energy balance	No
WaterGAP (19, 20) – Water – Global Analysis and Prognosis	No	Priestley-Taylor	β-Function	Degree day	No
WBM (21, 22) – Water Balance Model	No	Hamon	Saturation excess	Empirical temperature and precipitation-based formula	No

*Use of bulk transfer coefficients to calculate turbulent heat fluxes.
†Runoff is a nonlinear function of soil moisture.

1. Tang Q, Oki T, Kanae S, Hu H (2007) The influence of precipitation variability and partial irrigation within grid cells on a hydrological simulation. *J Hydrometeorol* 8(3):499–512.
2. Tang Q, Oki T, Kanae S, Hu H (2008) Hydrological cycles change in the Yellow River Basin during the last half of the 20th century. *J Clim* 21(8):1790–1806.
3. Hanasaki N, et al. (2008) An integrated model for the assessment of global water resources – Part 1: Model description and input meteorological forcing. *Hydrol Earth Syst Sci* 12(4): 1007–1025.
4. Hanasaki N, et al. (2008) An integrated model for the assessment of global water resources – Part 2: Applications and assessments. *Hydrol Earth Syst Sci* 12(4):1027–1037.
5. Best MJ, et al. (2011) The Joint UK Land Environment Simulator (JULES), model description – Part 1: Energy and water fluxes. *Geosci Model Dev.* 4(1):677–699.
6. Clark DB, et al. (2011) The Joint UK Land Environment Simulator (JULES), model description – Part 2: Carbon fluxes and vegetation dynamics. *Geosci Model Dev* 4(1):701–722.
7. Bondeau A, et al. (2007) Modelling the role of agriculture for the 20th century global terrestrial carbon balance. *Glob Change Biol* 13(3-4):679–706.
8. Rost S, et al. (2008) Agricultural green and blue water consumption and its influence on the global water system. *Water Resour Res* 44(9):W09405.
9. Gosling SN, Arnell NW (2011) Simulating current global river runoff with a global hydrological model: Model revisions, validation and sensitivity analysis. *Hydrol Processes* 25(7): 1129–1145.
10. Arnell NW (1999) A simple water balance model for the simulation of streamflow over a large geographic domain. *J Hydrol (Amst)* 217(3-4):314–335.
11. Pokhrel Y, et al. (2012) Incorporating anthropogenic water regulation modules into a land surface model. *J Hydrometeorol* 13(1):255–269.
12. Kumiko T, et al. (2003) Development of the minimal advanced treatments of surface interaction and runoff. *Global Planet Change* 38(1-2):209–222.
13. Hagemann S, Dümenil Gates L (2003) Improving a subgrid runoff parameterization scheme for climate models by the use of high resolution data derived from satellite observations. *Clim Dyn* 21(3-4):349–359.
14. Stacke T, Hagemann S (2012) Development and validation of a global dynamical wetlands extent scheme. *Hydrol Earth Syst Sci* 16(8):2915–2933.
15. Van Beek LPH, Wada Y, Bierkens MFP (2011) Global monthly water stress: I. Water balance and water availability. *Water Resour Res* 47(7):W07517.
16. Wada Y, et al. (2011) Global monthly water stress: II. Water demand and severity of water. *Water Resour Res* 47(7):W07518.
17. Lohmann D, Raschke E, Nijssen B, Lettenmaier DP (1998) Regional scale hydrology: I. Formulation of the VIC-2L model coupled to a routing model. *Hydrol Sci J* 43(1):131–141.
18. Liang X, Lettennmaier DP, Wood EF, Burges SJ (1994) A simple hydrologically based model of land surface water and energy fluxes for general circulation models. *J Geophys Res* 99 (D7):14415–14428.
19. Döll P, Kaspar F, Lehner B (2003) A global hydrological model for deriving water availability indicators: model tuning and validation. *J Hydrol (Amst)* 270(1-2):105–134.
20. Döll P, et al. (2012) Impact of water withdrawals from groundwater and surface water on continental water storage variations. *J Geodyn* 59–60:143–156.
21. Vörösmarty CJ, Peterson BJ, Lammers RB, Shiklomanov IA, Shiklomanov AI (1998) R-ArcticNET: A regional, electronic, hydrographic data network for the arctic region. University of New Hampshire, Durham, NH.
22. Wisser D, Fekete BM, Vörösmarty CJ, Schumann AH (2010) Reconstructing 20th century global hydrography: A contribution to the Global Terrestrial Network-Hydrology (GTN-H). *Hydrol Earth Syst Sci* 14(1):1–24.

Table S3. Overview and main characteristics of bio-geochemical models

Model name	Representation of dynamic vegetation	Represented bio-geochemical cycles
Hybrid (1)	Yes	Representation of C and N cycles (N provides constraints on photosynthesis, growth, and affects allocation of C to leaf area)
JeDI (2) – Jena Diversity Model	Yes	Representation of water and C cycle, no limitation of CO_2 fertilization by nutrient supply
JULES (3, 4) – Joint UK Land Environment Simulator	Yes	Representation of C cycle (no limitation of CO_2 fertilization by nutrient supply e.g., N or P)
LPJmL (5, 6) – Lund-Potsdam-Jena managed Land Dynamic Global Vegetation and Water Balance Model	Yes	Representation of a fully coupled water and carbon cycle (assuming optimal leaf nitrogen allocation, but no limitation of CO_2 fertilization by nutrient supply)
ORCHIDEE (7, 8)	Not in the configuration used for ISI-MIP	Representation of C cycle (no limitation of CO_2 fertilization by nutrient supply e.g., N or P) Land surface model – calculates energy fluxes and surface temperature on a 30-min time step
SDGVM (9, 10) – Sheffield Dynamic Vegetation Model	No	Fully coupled water and carbon cycle, below ground nitrogen cycle
VISIT (11, 12) – Vegetation Integrative Simulation for Trace gases	No	Representation of C and N cycle (but no limitation of CO_2 fertilization by N supply in this simulation). For vegetation processes, single vegetation-layer carbon cycle model.

ORCHIDEE, ORganizing Carbon and Hydrology in Dynamic EcosystEms.

1. Friend AD, White A (2000) Evaluation and analysis of a dynamic terrestrial ecosystem model under preindustrial conditions at the global scale. *Global Biogeochem Cycles* 14(4): 1173–1190.
2. Pavlick R, Drewry D, Bohn K, Reu B, Kleidon A (2012) The Jena Diversity-Dynamic Global Vegetation Model (JeDi-DGVM): A diverse approach to representing terrestrial biogeography and biogeochemistry based on plant functional trade-offs. *Biogeosciences Discuss* 9:4627–4726.
3. Best MJ, et al. (2011) The Joint UK Land Environment Simulator (JULES), model description – Part 1: Energy and water fluxes. *Geosci Model Dev* 4(1):677–699.
4. Clark DB, et al. (2011) The Joint UK Land Environment Simulator (JULES), model description – Part 2: Carbon fluxes and vegetation dynamics. *Geosci Model Dev* 4(1):701–722.
5. Sitch S, et al. (2003) Evaluation of ecosystem dynamics, plant geography and terrestrial carbon cycling in the LPJ dynamic global vegetation model. *Glob Change Biol* 9(2):161–185.
6. Gerten D, Schaphoff S, Haberlandt U, Lucht W, Sitch S (2004) Terrestrial vegetation and water balance—Hydrological evaluation of a dynamic global vegetation model. *J Hydrol (Amst)* 286(1):249–270.
7. Krinner G, et al. (2005) A dynamic global vegetation model for studies of the coupled atmosphere-biosphere system. *Global Biogeochem Cycles* 19(1):GB1015.
8. Piao S, et al. (2007) Changes in climate and land use have a larger direct impact than rising CO_2 on global river runoff trends. *Proc Natl Acad Sci USA* 104(39):15242–15247.
9. Le Quere C, et al. (2009) Trends in the sources and sinks of carbon dioxide. *Nat Geosci* 2(12):831–836.
10. Woodward FI, Smith TM, Emanuel WR (1995) A global land primary productivity and phytogeography model. *Global Biogeochem Cycles* 9(4):471–490.
11. Inatomi M, Ito A, Ishijima K, Murayama S (2010) Greenhouse gas budget of a cool temperate deciduous broadleaved forest in Japan estimated with a process-based model. *Ecosystems (N Y)* 13(3):472–483.
12. Ito A, Inatomi M (2012) Use of a process-based model for assessing the methane budgets of global terrestrial ecosystems and evaluation of uncertainty. *Biogeosciences* 9(2):759–773.

Table S4. Overview and main characteristics of malarial models

Model name	Input	Effect of rainfall	Effect of temperature	Output	Notes
LMM 205 (1, 2) – Liverpool Malaria Model	Monthly temperature and rainfall	Mosquito population based on rainfall in previous month	Biting rates, sporogonic cycle length, survival probability	Transmission based on reproduction ratio R_0, R_0 > 1 for sustainable disease transmission	Based on vector transmission potential model
MARA (3, 4) – Mapping Malaria Risk in Africa	Monthly temperature and rainfall	3-mo rainfall above minimum threshold, catalyst month with rainfall above a second threshold	Temperature above a threshold + a seasonality index based on SD of monthly rainfall	Malaria season in progress or not	Very simplified seasonal model of malaria transmission
MIASMA (5, 6) – Modeling Framework for the Health Impact Assessment of Man-Induced Atmospheric Changes	Temperature	Rainfall above minimum threshold	Effects on survival probability and biting frequency of mosquitoes	R_0 > 1 for sustainable disease transmission	Model not constrained by present day distribution of malaria vectors
VECTRI (7) - vector-borne disease community model of the International Centre for Theoretical Physics, Trieste	Daily temperature and rainfall	Physical model of surface pool hydrology: low rainfall increases breeding sites, high rainfall flushes larva	Sporogonic and gonotrophic cycle development rates, mortality rates for adult vectors, growth rate and mortality of larvae (water temperature)	Daily number of infectious bites by infectious vectors, transmission probability per person per day	Accounts for human population density in the calculation of biting rates, full dynamic model with daily timestep and accounting for subseasonal variations in climate

1. Hoshen MB, Morse AP (2004) A weather-driven model of malaria transmission. *Malar J* 3(32):32.
2. Jones AE, Morse AP (2010) Application and validation of a seasonal ensemble prediction system using a dynamic malaria model. *J Clim* 23(15):4202–4215.
3. Craig MH, Snow RW, Le Sueur D (1999) A climate based distribution model of malaria transmission in Sub-Saharan Africa. *Parasitology Today* 15(3):104.
4. Jones A (2007) Seasonal ensemble prediction of malaria in Africa. PhD thesis (University of Liverpool, Liverpool, UK).
5. Van Lieshout M, Kovats RS, Livermore MTJ, Martens P (2004) Climate change and malaria: Analysis of the SRES climate and socio-economic scenarios. *Glob Environ Change* 14(1):87–99.
6. Martens P (1999) MIASMA: Modelling framework for the health Impact Assessment of Man-induced Atmospheric changes. *Electronic Series on Integrated Assessment Modeling (ESIAM) 2*.
7. Tompkins AM, Ermert V (2013) A regional-scale, high resolution dynamical malaria model that accounts for population density, climate and surface hydrology. *Malar J* 12:65.